PHOTOSYNTHESIS

Quieting a noisy antenna reproduces photosynthetic light-harvesting spectra

Trevor B. Arp[1,2]*, Jed Kistner-Morris[1,2]*, Vivek Aji[2], Richard J. Cogdell[3,4]†, Rienk van Grondelle[4,5]†, Nathaniel M. Gabor[1,2,4]†

Photosynthesis achieves near unity light-harvesting quantum efficiency yet it remains unknown whether there exists a fundamental organizing principle giving rise to robust light harvesting in the presence of dynamic light conditions and noisy physiological environments. Here, we present a noise-canceling network model that relates noisy physiological conditions, power conversion efficiency, and the resulting absorption spectra of photosynthetic organisms. Using light conditions in full solar exposure, light filtered by oxygenic phototrophs, and light filtered under seawater, we derived optimal absorption characteristics for efficient solar power conversion. We show how light-harvesting antennae can be tuned to maximize power conversion efficiency by minimizing excitation noise, thus providing a unified theoretical basis for the observed wavelength dependence of absorption in green plants, purple bacteria, and green sulfur bacteria.

In photosynthesis, light energy harvesting begins with the absorption of sunlight. Photoexcitation energy is rapidly transferred through an antenna network before reaching the reaction center, where charge transfer converts excitation energy into an electrochemical potential gradient across the photosynthetic membrane (*1*). Even in the presence of dynamic light conditions, rapidly fluctuating molecular structure, and highly intricate energy transfer pathways (*1*–*5*), the light-to-electron conversion process exhibits near unity quantum efficiency. The delicate interplay of quantum effects with molecular mechanisms of energy management, e.g., nonphotochemical quenching (*6*–*8*), has been explored across diverse phototrophs (*9*–*12*) but the elementary connection between highly robust light energy harvesting and energetic fluctuations has not been established.

Transforming noisy inputs into quiet outputs represents a general design challenge in network architectures including multinational energy grids (*13*–*17*), auditory and visual neural networks (*18*–*21*), and nanoscale photocells for next-generation optoelectronics (*22*). Although network inputs exhibit statistical fluctuations (e.g., rapid changes of sunlight absorbed by a leaf or solar panel), network outputs may demand a steady rate of information or energy for optimal performance (e.g., constant power from the grid to maintain indoor lighting). Statistical fluctuations—arising from environmental variations and internal processes—fundamentally limit the throughput efficiency of any network. If the flow of energy (power) into a network is substantially larger or smaller than the flow out of the network required to optimally match the output demand, then the network must adapt or be structured in such a way as to reduce the sudden overflow or underflow of energy. When the network fails to manage fluctuations, the results may be extraordinary (e.g., photo-oxidative stress in photosynthetic light harvesting or explosive damage to transformers caused by fluctuations in the grid).

We constructed a model that uses generalizations of networks to extract essential aspects of photosynthetic light harvesting (Fig. 1). A simple network of nodes (points at which lines intercept) connected by links (connecting lines) represent physical objects: excitation energy levels and intermolecular transfer events within the antenna system, respectively. In photosynthesis, light enters the antenna through a large number of pigment molecules, each of which is a member of a small set of distinct molecular species (e.g., chlorophyll a and b). Our model considers the advantage in having light entering the network through two classes of absorbing excitation energy levels, nodes A and B, which can absorb powers $\mathcal{P}_A$ and $\mathcal{P}_B$.

After an absorption event, excitation energy moves between internal nodes of the antenna network, representing the excitation of intermediate states within the biological antenna complex (*2*, *11*, *23*). As an example, excitation energy absorbed by a chlorophyll b molecule in the light-harvesting complex LHC2 is transferred to chlorophyll a, and from there to another chlorophyll a in the same or in another complex. There are many such pathways through the antenna network that may share intermediate links, but each specific pathway (Fig. 1A, colored lines) eventually terminates on the output, O, which on average delivers power Ω. Rather than model each pathway, we modeled the average behavior from all inputs A and B through all pathways in the network. Thus, we define probabilities p_A and p_B, which are the total probabilities that any input A and B will absorb. Mathematically, the example pathway given above, along with all other

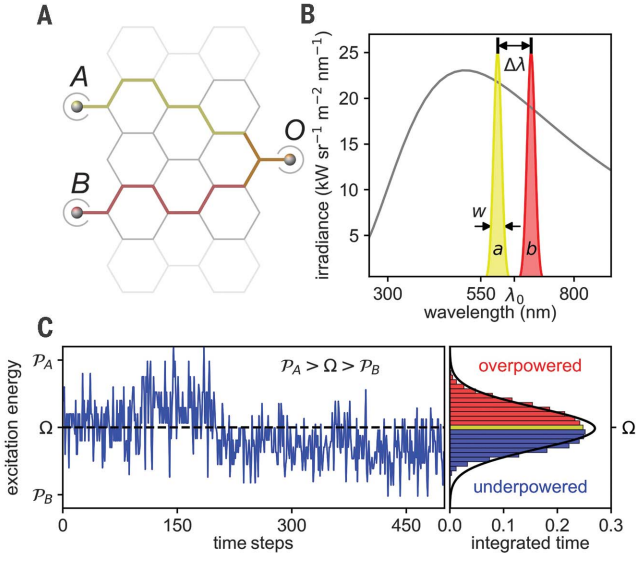

Fig. 1. Light-harvesting noisy antenna. (**A**), Schematic of a photosynthetic antenna reduced into a network with two input nodes A and B with input rates $\mathcal{P}_A$ and $\mathcal{P}_B$ and output O with rate Ω. Energy is absorbed by molecules a and b (at rates $\mathcal{P}_A$ and $\mathcal{P}_B$) and is transferred to the output as usable energy. (**B**) Schematic two-channel antenna absorption spectra (yellow and red) and incident blackbody light source (gray). The quantities λ_0, $\Delta\lambda$, and w are, respectively, the center wavelength, distance between peaks, and width of the absorption peaks. (**C**) (Left) Simulated average excitation energy as a function of time within a noisy antenna composed of 10 sets of a and b molecules. (Right) Time-averaged histogram of the internal energy (detailed in the supplementary materials, section S1.4). The antenna is subject to internal (fast) and external (slow) fluctuations. Over long time scales, the time-averaged histogram resembles a normal distribution (black line).

[1]Laboratory of Quantum Materials Optoelectronics, University of California, Riverside, CA 92521, USA. [2]Department of Physics and Astronomy, University of California, Riverside, CA 92521, USA. [3]Institute of Molecular, Cell, and Systems Biology, College of Medical, Veterinary, and Life Sciences, University of Glasgow, Glasgow G128QQ, UK. [4]Canadian Institute for Advanced Research, Toronto, Ontario M5G 1M1, Canada. [5]Department of Physics and Astronomy, Faculty of Sciences, Vrije Universiteit Amsterdam, 1081 HV Amsterdam, Netherlands.
*These authors contributed equally to this work
†Corresponding author. Email: richard.cogdell@glasgow.ac.uk (R.C.); r.van.grondelle@vu.nl (R.v.G.); nathaniel.gabor@ucr.edu (N.M.G.)

pathways that originate on a node B, is contained in p_B. The average power (or rate of energy) coming from the B absorbers is therefore $p_B\mathcal{P}_B$. This is the average value; the actual flow of excitation energy at any given time is stochastic.

By analyzing the stochastic flow of excitation energy, we can characterize the antenna network by statistical averages (power throughput) and fluctuations in the rate of energy flow, which we will call noise (see the supplementary materials, section S1). The power throughput of the antenna system is determined by the external light conditions, the absorption characteristics of the absorbing pigment molecules (Fig. 1B) or input nodes, and the molecular dynamics of the network. The antenna inputs are described in the usual way: Light absorption by the pigment molecules is characterized by peak width w, separation $\Delta\lambda = |\lambda_B - \lambda_A|$, and the center wavelength (or average distance) between the peaks λ_0. The solar spectral irradiance (Fig. 1B, gray line), which varies as light propagates through air, the canopy, or seawater, gives the average power available within a given range of wavelengths. Choosing the wavelength of an absorption peak simultaneously specifies both the excitation energy and power entering the noisy antenna. Although the excitation energy is inversely proportional to wavelength, the absorbed power $\mathcal{P}_A$ or $\mathcal{P}_B$ is the integrated product of the spectral irradiance and the absorption characteristics of the light-harvesting antenna.

Because the absorbed solar power rarely matches exactly the rate of optimal output, a finely tuned network is one that most effectively balances minimizing the internal noise with robustness against external noise. Noise in the antenna arises from two main sources: inherent mismatch between inputs and output, which may arise because of fast dynamics in the protein structure and corresponding electronic properties, and dynamic external light conditions. In photosynthesis, an overpowered antenna will produce excess energy that can drive deleterious back reactions (*24*, *25*). Conversely, a light-harvesting network in an underpowered state produces nonoptimal output, because the rate of energy transfer out of the network is fixed by electrochemical processes (*26*). Over long periods of time, the degree to which the light-harvesting network is overpowered or underpowered is measured by the mean-squared deviation (i.e., noise) of the total input power (through $\mathcal{P}_A$ and $\mathcal{P}_B$) from the optimal output power at Ω, (Fig. 1C) (see the supplementary materials, section S1).

Tuning only the absorption characteristics, our goal was to find a network that spends the least amount of time in a state for which the input power is too large or too small compared with the output of the network, thus maximizing power conversion efficiency (Fig. 1C). Within our model, probabilities p_A and p_B couple the inputs of the network $\mathcal{P}_A$ and $\mathcal{P}_B$ to the output Ω: $p_A\mathcal{P}_A + p_B\mathcal{P}_B = \Omega$. From this expression, we first evaluate the variance of the average distribution $p_A\mathcal{P}_A + p_B\mathcal{P}_B$. Minimizing this variance yields the optimal values of $\mathcal{P}_A$ and $\mathcal{P}_B$ to quiet the antenna. We then input the local spectral irradiance to a model optimization function, the maxima of which determine the optimal absorption characteristics for noise cancellation (see the supplementary materials, sections S1.1 to S1.3).

Using this framework, we can predict the behavior of three noise regimes within the antenna network: overtuned, finely tuned, and poorly tuned (Fig. 2). For simplicity, these examples are where $\Omega = (\mathcal{P}_A + \mathcal{P}_B)/2$, whereas a broader parameter range is explored in detail in the supplementary materials, section S1.2. Although the light conditions are identical for all three cases (Fig. 2A, gray lines), we can examine how the noise changes with different absorption characteristics (details of this calculation can be found in the supplementary materials, section S1.4). When the absorbing peaks are spaced too closely (Fig. 2A, top), the inherent antenna noise can be strongly reduced, and in the limit that $\mathcal{P}_A = \Omega = \mathcal{P}_B$, there

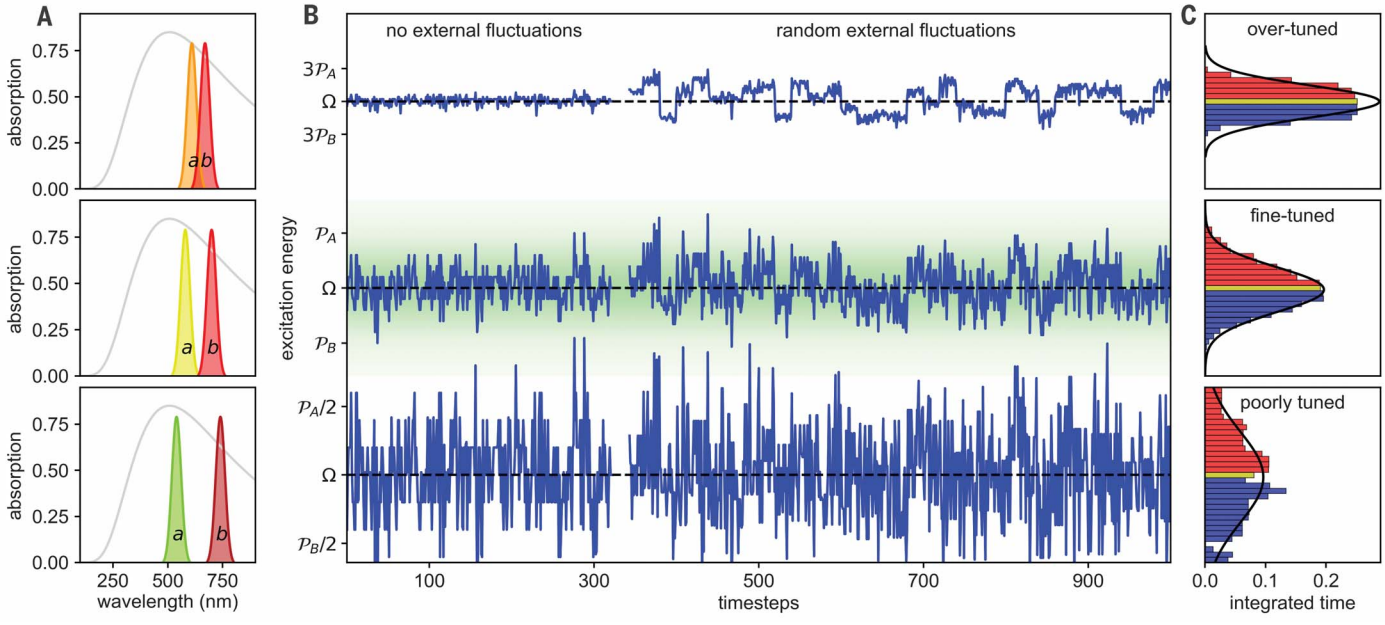

Fig. 2. Quieting a noisy antenna by tuning the absorption characteristics. (**A**) Absorption peaks for two absorbers *a* and *b* overlaid on an ideal blackbody solar spectrum (T = 5500 K, gray line) for three cases: two closely spaced absorbers (top), two absorbers separated to optimize the noisy antenna (middle), and two widely separated absorbers (bottom). (**B**) Simulated excitation energy versus time for a two-channel antenna with three different values of Δ, comparable to the cases shown in (A). The left side shows the excitation energy time traces without external fluctuations. The right side includes random external fluctuations. (**C**) Histograms of time spent in overpowered (red) and underpowered (blue) states for the three series in (B). In the top panel, the distribution is flat and favors no value. In the middle panel, the distribution is a sharply peaked normal distribution that favors Ω. In the bottom panel, the distribution is normal but wider than that in the middle panel.

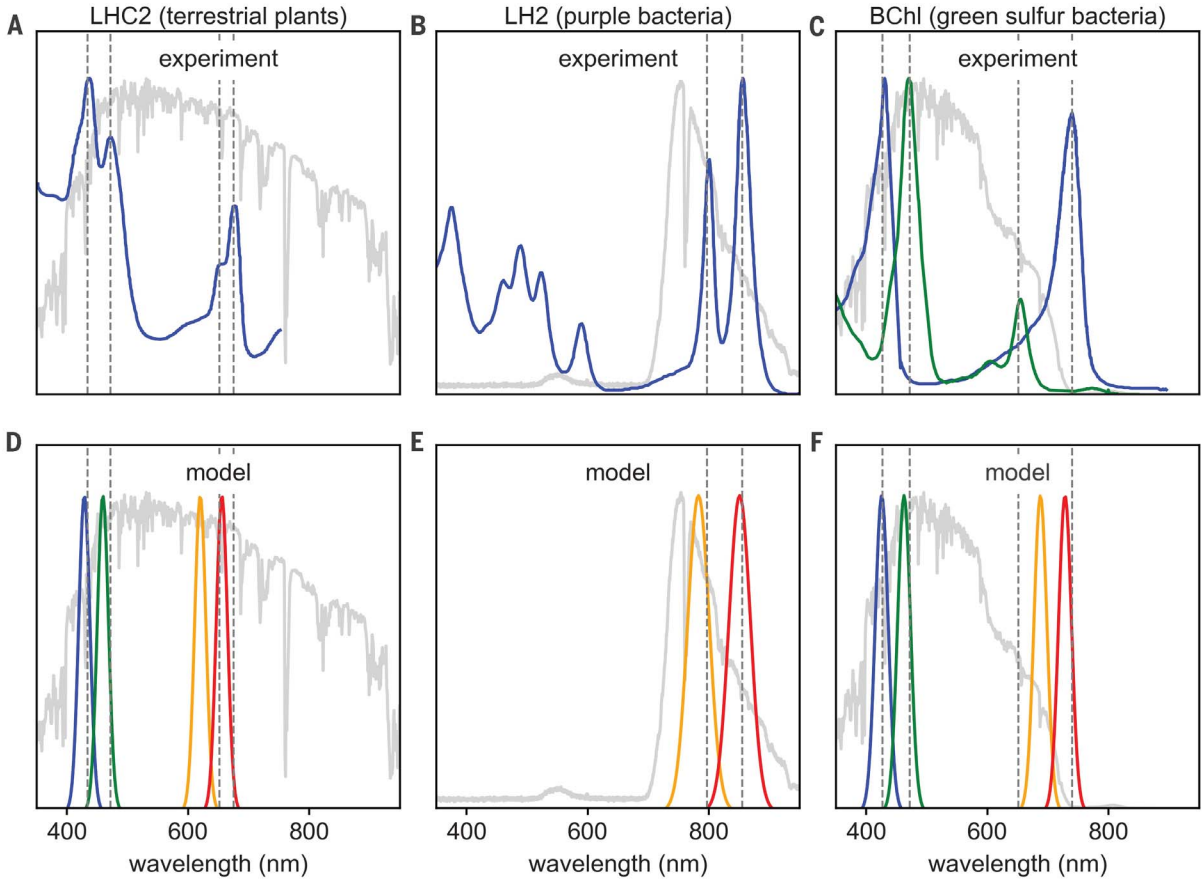

Fig. 3. Comparison of the noisy antenna model with photosynthetic absorption spectra in three distinct niches. (**A**) Absorption spectrum of LHC2 (blue) (*27*) overlaid on the terrestrial solar spectrum (light gray) (*31*). (**B**) Absorption spectrum of the LH2 complex (*28*) overlaid on the solar spectrum measured below a canopy of leaves (light gray) (see the supplementary materials, section S3, for details). (**C**) Absorption spectra of bacteriochlorophyll c (blue) and e (green) (*29*, *30*) compared with the calculated solar spectrum at a 2-m depth of water (light gray) (*32*, *33*). (**D** to **F**) Predicted ideal absorption peaks from optimizing $\Delta = \mathcal{P}_A - \mathcal{P}_B$ for the full solar spectrum, the solar spectrum attenuated through canopy, and the solar spectrum attenuated through seawater, respectively (see the supplementary materials, sections S2 and S3, for optimization and spectra details, respectively). Photosynthetic absorption peaks are identified with dashed lines.

are negligible fluctuations in the rate of energy flow (Fig. 2B, top left). This lower bound to the internal noise cannot be reached in natural photosynthetic antennae, where protein dynamics will always drive fluctuations of intermediate excitation energy transfer events. Rather, the overtuned antenna noise is directly proportional to, and thus dominated by, changes in the varying light spectrum (Fig. 2B, top right). In the presence of random external fluctuations, the distribution of time spent in an overpowered or underpowered state is flat (Fig. 2C, top). In the overtuned antenna, the average input rarely matches the optimal output.

A poorly tuned antenna (Fig. 2A, bottom) is similarly deficient. If the absorbing peaks are well separated, then the antenna spends most of the time overpowered or underpowered. When the power sources $\mathcal{P}_A$ or $\mathcal{P}_B$ are significantly greater or less than the power sink ($\mathcal{P}_A >> \Omega >> \mathcal{P}_B$), the noise (as evidenced by a histogram of the excitation energy) in the poorly tuned antenna becomes broader as the absorbing peaks become more separated (Fig. 2C, bottom). When viewed over long times, the poorly tuned antenna spends too little time outputting the optimal power Ω.

The finely tuned antenna absorbs at specific positions on the spectrum that give rise to robust light harvesting even in the presence of both varying light conditions and substantial internal noise. Compared with the overtuned and undertuned cases, the finely tuned antenna allows for intermediate internal noise levels (Fig. 2B, middle) yet delivers a narrow distribution of power centered at the optimal output Ω (Fig. 2C, middle). Robustness in light harvesting is thus the ability to output, on average, the optimal rate Ω yet simultaneously allow for internal noise.

To determine the optimal absorption spectrum for robust light harvesting, we computed the spectral positions for which the peaks are as close as possible on the light spectrum (favoring reduced internal noise) yet the difference in the absorbed power $\Delta = \mathcal{P}_A - \mathcal{P}_B$ is maximized (supporting robustness against external variations). This condition is equivalent to maximizing the derivative of the light spectrum with respect to wavelength, thus resulting in absorption peaks in regions of steepest slope (see the supplementary materials, section S1.3). The absorption spectra, and thus the excitation transitions, are tuned so that the time-averaged sum of input excitation energy is sharply peaked at the output rate (Fig. 2C, middle).

For three prototypical photosynthetic antennae, the light-harvesting complex of green plants (LHC2), the light-harvesting complex of purple bacteria (LH2), and the bacteriochlorophyll c and e pigments of green sulfur bacteria (BChl c and e), the natural absorption spectrum (Fig. 3, A to C) (*27*–*30*) can be compared with that predicted by our model

(Fig. 3, D to F) (see the supplementary materials, section S2, for full details), which takes as input the local irradiance spectrum, shown as solid gray lines in Fig. 3, A to F. The absorption peak positions and spectral separation predicted under light conditions in air (*31*), under canopy, or under seawater (*32*, *33*) (colored lines in Fig. 3, D, E, and F, respectively) show strong agreement with the absorption spectra of these three phototrophs. Using only the external light spectrum and the linewidth w, the predicted peak center position λ_0 and separation $\Delta\lambda$ reproduced the measured absorption peaks with an average error of 2.1% (Table 1).

The noisy antenna model also reproduced a general feature of photosynthetic light harvesting that was observed across all three prototypical phototrophs. Photosynthetic pigments do not absorb at the maximum solar power. Instead, all three phototrophs considered exhibit pairs of closely spaced peaks in regions where the spectrum shows a steep rate of change with respect to wavelength. Photosynthetic plants look green because their antenna complexes absorb light across the visible spectrum, including the blue and red portions, yet reflect green wavelengths (Fig. 3D). Purple bacteria are aquatic phototrophs (*34*). They have adapted to sunlight that is filtered through the canopy of trees and floating aerobic phototrophs (Fig. 3E, gray line, and see the supplementary materials, section S3) and use a light-harvesting complex in which bacteriochlorophyll dominates light absorption away from the visible, including green (Fig. 3E). Green sulfur bacteria are a geographically diverse group of bacteria that are adapted to solar light shining through seawater to depths where it is anaerobic (*35*). They do not absorb the peak intensity of this attenuated light spectrum and instead absorb in the region of steepest spectral rate of change.

Underwater phototrophs provide an excellent natural experiment with which to test the predictive strength of our model because the solar spectrum is highly variable as a function of depth (*36*). When considering the penetrating spectrum below the seawater surface, light intensity is attenuated as depth increases, particularly in the red and infrared zones, because of absorption and scattering in seawater (Fig. 4A). By comparing the absorption spectra of subsurface marine phototrophs, such as green sulfur bacteria, with those predicted by quieting a noisy antenna, we can explore whether the natural photosynthetic absorption spectrum matches our model predictions for the relevant phototroph's preferred depth.

From these attenuated solar spectra, we calculated an optimization parameter Δ^{op} as a function of $\Delta\lambda$ and λ_0. Δ^{op} is a function modified from the calculation of $\Delta = \mathcal{P}_A - \mathcal{P}_B$ such

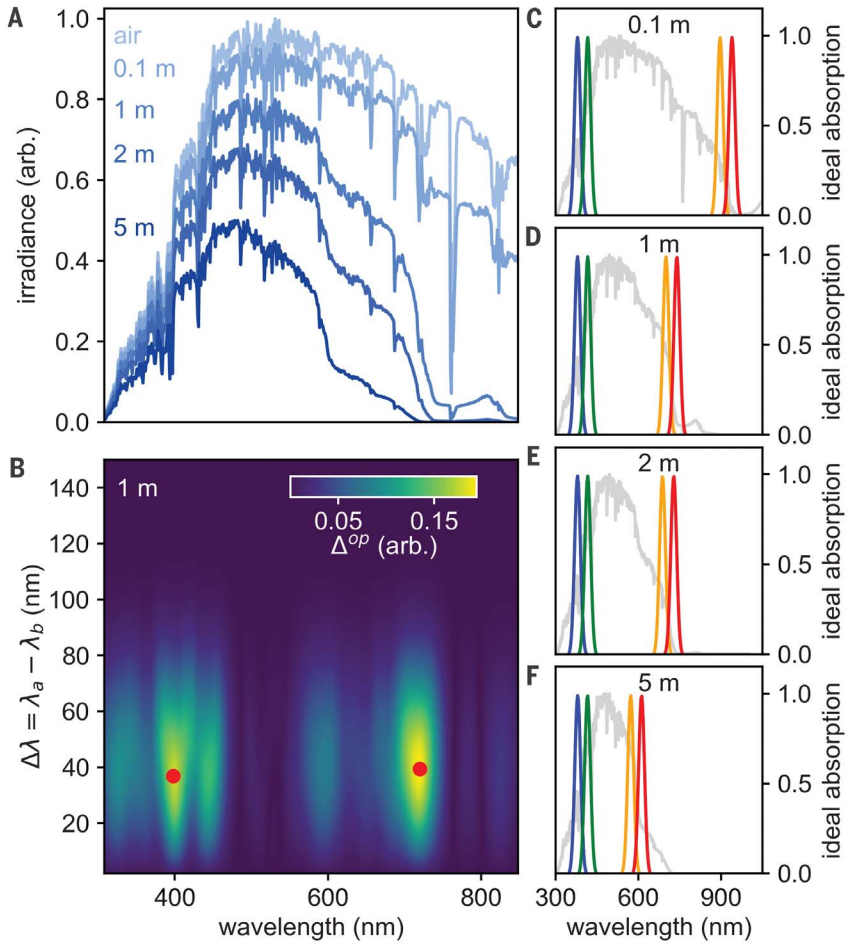

Fig. 4. Predicted absorption spectra of a finely tuned noisy antenna under seawater. (**A**) Solar spectrum in air (*31*) and attenuated by various depths of water (labeled) (*32*, *33*). (**B**) Optimization landscape calculation of Δ^{op} versus center wavelength λ_0 and peak separation $\Delta\lambda$ for the solar spectrum under 1 m of seawater (w = 15 nm). Red points identify two equally favorable maxima corresponding to a set of peaks on either side of the spectral maximum. (**C** to **F**) Ideal absorption peaks predicted from the solar spectrum at each depth. (D) shows the peaks extracted from the calculation in (B) color coded blue, green, orange, and red to track peak locations with depth.

Table 1. Absorption peak data versus model calculation.

Peak name	Actual value, nm (eV)	Calculated value, nm (eV)	Relative % error from nm (eV)	Reference
Chlorophyll a 1	428 (2.90)	429 (2.89)	0.23 (0.34)	(*27*)
Chlorophyll b 1	440 (2.82)	459 (2.70)	4.32 (4.26)	(*27*)
Chlorophyll b 2	652 (1.90)	620 (2.00)	4.91 (5.26)	(*27*)
Chlorophyll a 2	660 (1.88)	656 (1.89)	0.61 (0.53)	(*27*)
LH2 band 1	801 (1.55)	783 (1.58)	2.25 (1.94)	(*28*)
LH2 band 2	857 (1.45)	851 (1.46)	0.70 (0.69)	(*28*)
Bacteriochlorophyll c 1	431 (2.88)	426 (2.91)	1.16 (1.04)	(*29*)
Bacteriochlorophyll e 1	461 (2.69)	462 (2.68)	0.22 (0.37)	(*30*)
Bacteriochlorophyll e 2	655 (1.89)	688 (1.80)	5.04 (4.76)	(*30*)
Bacteriochlorophyll c 2	740 (1.68)	728 (1.70)	1.62 (1.19)	(*29*)

that its maxima quiet a noisy antenna (see the supplementary materials, section S1.3). An example color map of the magnitude of Δ^{op} at a depth of 1 m and w = 15 nm reveals two maxima in the color plot near λ_o = 400 and 750 nm (Fig. 4B). These maxima identify the wavelength characteristics of a finely tuned antenna under seawater. By extracting the values of $\Delta\lambda$ and λ_o at the maximum in Δ, we obtain the characteristic absorption spectra of the fine tuned antenna as a function of seawater depth (Fig. 4, C to F). We found that quieting a noisy antenna under 2 m of seawater accurately reproduces the absorption spectrum of green sulfur bacteria. Although highly adaptable, green sulfur bacteria are known to thrive at 1 to 2 m below the surface (*37*), coinciding with the conditions for which their light-harvesting antenna is finely tuned for solar power conversion.

The degree to which we were able to reproduce photosynthetic absorption spectra is a surprising result, suggesting an underlying organizing principle for light-harvesting systems: Fluctuations fundamentally limit the efficiency of networks and must be avoided. Phototrophs must balance environmental inputs to sustain steady production and storage of fuel under substantially different environmental conditions. Phototrophs across many photosynthetic niches may have adapted to build fluctuation-canceling light-harvesting antennae onto which other active mechanisms for reducing fluctuations can be added (e.g., nonphotochemical quenching) (*6*–*8*). Although the connection of our model to natural antenna systems requires detailed quantum models, our framework gives new insight into how extinction coefficients, delocalization lengths, and radiative rates conspire to reduce noise in natural antennae. Moreover, our findings will inspire comprehensive experiments in which the light environment is carefully controlled while the absorption spectrum of adaptable model organisms is monitored. By developing noise-canceling antennae as a technological foundation, natural and artificial energy-harvesting networks—from bacteria thriving underwater to extended power grids—could be adapted to efficiently convert noisy inputs into robust outputs.

REFERENCES AND NOTES

1. R. Blankenship, *Molecular Mechanisms of Photosynthesis* (Wiley, 2002).
2. R. van Grondelle, J. P. Dekker, T. Gillbro, V. Sundstrom, *Biochim. Biophys. Acta.* **1187**, 1–65 (1994).
3. G. P. van Nieuw Amerongen, S. van Delft, M. A. Vermeer, J. G. Collard, V. W. M. van Hinsbergh, *Circ. Res.* **87**, 335–340 (2000).
4. G. D. Scholes, G. R. Fleming, A. Olaya-Castro, R. van Grondelle, *Nat. Chem.* **3**, 763–774 (2011).
5. R. Croce, H. van Amerongen, *Nat. Chem. Biol.* **10**, 492–501 (2014).
6. C. Külheim, J. Agren, S. Jansson, *Science* **297**, 91–93 (2002).
7. A. A. Pascal *et al*., *Nature* **436**, 134–137 (2005).
8. A. V. Ruban *et al*., *Nature* **450**, 575–578 (2007).
9. R. G. Fleming, R. van Grondelle, *Phys. Today* **47**, 48–55 (1994).
10. E. Romero, V. I. Novoderezhkin, R. van Grondelle, *Nature* **543**, 355–365 (2017).
11. T. Mirkovic *et al*., *Chem. Rev.* **117**, 249–293 (2017).
12. G. D. Scholes *et al*., *Nature* **543**, 647–656 (2017).
13. K. Schmietendorf, J. Peinke, O. Kamps, *Eur. Phys. J. B* **90**, 222 (2017).
14. B. Schäfer, C. Beck, K. Aihara, D. Witthaut, M. Timme, *Nat. Energy* **3**, 119–126 (2018).
15. T. Nesti, A. Zocca, B. Zwart, *Phys. Rev. Lett.* **120**, 258301 (2018).
16. H. Haehne, J. Schottler, M. Waechter, J. Peinke, O. Kamps, *Europhys. Lett.* **121**, 30001 (2018).
17. T. Coletta, B. Bamieh, P. Jacquod, Transient performance of electric power networks under colored noise. arXiv:1807.09048v2 [math.OC] (31 January 2019).
18. D. De Ridder *et al*., *Neurosci. Biobehav. Rev.* **44**, 16–32 (2014).
19. A. M. Leaver *et al*., *Neuron* **69**, 33–43 (2011).
20. B. B. Averbeck, P. E. Latham, A. Pouget, *Nat. Rev. Neurosci.* **7**, 358–366 (2006).
21. I. Kanitscheider, R. Coen-Cagli, A. Pouget, *Proc. Natl. Acad. Sci. U.S.A.* **112**, E6973–E6982 (2015).
22. T. B. Arp, Y. Barlas, V. Aji, N. M. Gabor, *Nano Lett.* **16**, 7461–7466 (2016).
23. R. van Grondelle, *Biochim. Biophys. Acta* **811**, 147–195 (1985).
24. P. Horton, A. V. Ruban, R. G. Walters, *Annu. Rev. Plant Physiol. Plant Mol. Biol.* **47**, 655–684 (1996).
25. A. V. Ruban, M. P. Johnson, C. D. P. Duffy, *Biochem. Biophys. Acta.* **1817**, 167–181 (2012).
26. G. D. Farquhar, S. von Caemmerer, J. A. Berry, *Planta* **149**, 78–90 (1980).
27. T. P. J. Krüger, R. van Grondelle, *Physica B* **480**, 7–13 (2016).
28. R. J. Cogdell *et al*., *FEBS Lett.* **555**, 35–39 (2003).
29. D. C. Brune, T. Nozawa, R. E. Blankenship, *Biochemistry* **26**, 8644–8652 (1987).
30. C. M. Borrego, J. B. Arellano, C. A. Abella, T. Gillbro, J. Garcia-Gil, *Photosynth. Res.* **60**, 257–264 (1999).
31. National Renewable Energy Laboratory (NREL), U.S. Department of Energy, *Reference Air Mass 1.5 Spectra* (2003); https://www.nrel.gov/grid/solar-resource/spectra-am1.5.html.
32. H. Buiteveld, J. H. M. Hakvoort, M. Donze, "Optical properties of pure water," in *Proceedings of SPIE 2258 Ocean Optics XII* (26 October 1994), pp. 174–183; https://doi.org/10.1117/12.190060.
33. L. Kou, D. Labrie, P. Chylek, *Appl. Opt.* **32**, 3531–3540 (1993).
34. C. N. Hunter, F. Daldal, M. C. Thurnauer, J. T. Beatty, *The Purple Phototropic Bacteria* (Springer, 2009).
35. J. M. Olsen, in *Green Photosynthetic Bacteria*, J. M. Olsen, J. G. Ormerod, J. Amesz, E. Stackebrandt, H. G. Trüper, Eds. (Springer, 1988), pp. 315–319.
36. P. Jenkins *et al*., *IEEE J. Photovoltaics* **4**, 202–207 (2014).
37. A. Kharcheva, A. Zhiltsova, in *WDS'16 Proceedings of Contributed Papers – Physics*, J. Šafránková and J. Pavlů, Eds. (Matfyzpress, 2016); pp. 214–218.
38. T. B. Arp, qmolabucr/qntenna: Publication Release, version v1.1, Zenodo (2020); https://doi.org/10.5281/zenodo.3765834.

ACKNOWLEDGMENTS

We thank V. Elser, J. Iezzi, P. McEuen, T. Sargent, and C. Varma for valuable discussions. **Funding:** T.B.A., J. K.-M., and N.M.G were supported by the Air Force Office of Scientific Research Young Investigator Program (YIP) award no. FA9550-16-1-0216, National Science Foundation Division of Materials Research CAREER award no. 1651247, and the U.S. Department of the Navy Historically Black Colleges, Universities and Minority Serving Institutions (HBCU/MI) award no. N00014-19-1-2574. N.M.G. acknowledges support from a Cottrell Scholar Award and a Canadian Institute for Advanced Research (CIFAR) Azrieli Global Scholar Award. T.B.A. acknowledges support from the Fellowships and Internships in Extremely Large Data Sets (FIELDS) program, a NASA MUREP Institutional Research Opportunity (MIRO) program grant no. NNX15AP99A. R.J.C. gratefully acknowledges support from the Photosynthetic Antenna Research Center, an Energy Frontier Research Center funded by the U.S. Department of Energy, Office of Science, Office of Basic Energy Sciences under award no. DE-SC 0001035 and the Biotechnological and Biological Sciences Research Council (BBSRC). R.v.G. was supported by the Royal Netherlands Academy of Arts and Sciences and the Canadian Institute for Advanced Research (CIFAR). **Author contributions:** T.A. and J. K. M. performed detailed analysis and computational modelling. N.M.G. and V.A. conceived the conceptual model and supervised the analytical and computational modeling with additional input from R.J.C. and R.v.G. R.J.C., N.M.G., and R.v.G. chose which phototrophs should be used as exemplars. All authors contributed to the writing of the manuscript. **Competing interests:** The authors declare no competing interests. **Data and materials availability:** The code for the parameter search that generates the main results shown in Figs. 3 and 4, as well as the discrete simulation code used to generate Figs. 1C and 2B, are available on Zenodo (*38*). This repository includes the irradiance data shown in Fig. 3, D to F, and Fig. 4A such that all model results can be fully replicated.

SUPPLEMENTARY MATERIALS

science.sciencemag.org/content/368/6498/1490/suppl/DC1
Materials and Methods
Supplementary Text
Figs. S1 to S14
References (*39*–*59*)
MDAR Reproducibility Checklist

View/request a protocol for this paper from *Bio-protocol*.

20 December 2019; accepted 4 May 2020
10.1126/science.aba6630

Quieting a noisy antenna reproduces photosynthetic light-harvesting spectra

Trevor B. Arp, Jed Kistner-Morris, Vivek Aji, Richard J. Cogdell, Rienk van Grondelle and Nathaniel M. Gabor

Science **368** (6498), 1490-1495.
DOI: 10.1126/science.aba6630

Pairs of peaks stabilize output power

A counterintuitive feature of photosynthesis is that the primary pigments involved in absorbing light—for example, chlorophyll a and b in plants—do not all absorb right at the peak of the spectrum but instead are offset from the peak and each other. Arp *et al.* formulated a network model that explains how using pigments with this absorption-peak pattern can mitigate internal and external fluctuations in energy transfer, minimizing noise in output power (see the Perspective by Duffy). The model accurately reproduces absorption peaks for three diverse photosynthetic systems from different spectral environments. Such a mechanism may provide an underlying robustness to biological photosynthetic processes that can be further tuned and tweaked to adapt to longer-scale fluctuations in light intensity.

Science, this issue p. 1490; see also p. 1427

Science (print ISSN 0036-8075; online ISSN 1095-9203) is published by the American Association for the Advancement of Science, 1200 New York Avenue NW, Washington, DC 20005. The title *Science* is a registered trademark of AAAS.